



New and innovative microwave-assisted technology for synthesis of guar gum-grafted acrylamide hydrogel superabsorbent for the removal of acid red 8 dye from industrial wastewater

Mervette El Batouti¹ · Wagih Sadik² · Abdel Ghaffar Eldemerdash² · Esra Hanafy² · Howida Abouel Fetouh¹

Received: 24 July 2021 / Revised: 12 March 2022 / Accepted: 15 April 2022 /

Published online: 9 June 2022

© The Author(s) 2022

Abstract

The goal of this study is to develop a new effective guar gum-grafted acrylamide hydrogel for wastewater treatment, abbreviated as (guar gum-g-acrylamide). For the non-biodegradable and hazardous synthetic acid red 8, the produced guar gum-g-acrylamide hydrogel is a promising thermally stable adsorbent. Microwave-aided technique, ammonium persulfate initiator, and *N,N'*-methylene-bis-acrylamide cross-linker are used to make a hydrogel comprising natural polysaccharides guar gum grafted by poly acrylamide. Fourier transformer infrared (FTIR) spectra and scanning electron microscopy (SEM) demonstrate that varied percentages of acrylamide successfully graft the backbone of guar gum. When the grafting percentage of acrylamide is raised, the hydrogel's maximum adsorption capacity (q_e) increases. At pH 1 of dye solution, maximum adsorption capacity (q_e) is 18 mg.g⁻¹, at pH 9; q_e is decreased up to 8 mg.g⁻¹. At 0.5 g.L⁻¹ hydrogel, the dye has a low removal percentage (34%), but when the hydrogel dosage is increased to 8 g.L⁻¹, the removal percentage increases to 90%. When the initial AR8 dye concentration was increased from 50 to 300 mg.L⁻¹, the removal percentage reduced to 20% and the adsorbed quantity dye increased from 17 to 44 mg.g⁻¹, but both parameters became limited above this dye concentration. Other ideal conditions for AR8 dye removal by the hydrogel include 60 min of contact time, 150 revolutions per minute (rpm), and a temperature of 20 degrees Celsius. The AR8 dye adsorption kinetic is pseudo-second order, assuming electrostatic interaction between the negatively charged AR8 dye molecules and the positively charged hydrogel-functional group. The adsorption values fit the Langmuir isotherm, with q_{max} of 54.054 mg.g⁻¹. The adsorbed quantity (q_e) decreases as the temperature rises, indicating that dye molecules physisorbed on the hydrogel pores, and the maximum adsorption capacity is at 20 °C. The exothermic and spontaneity of adsorption were confirmed by the negative values of heat of adsorption (ΔH°_{ads}) and standard Gibbs free energy of adsorption

Extended author information available on the last page of the article

($\Delta G^{\circ}_{\text{ads}}$). The reusability of the hydrogel was validated after three cycles of desorption of AR8 dye from the hydrogel surface in alkaline solution.

Keywords Acid red 8 dye · Hydrogel · Grafting · Adsorption · Adsorption capacity · Removal percentage

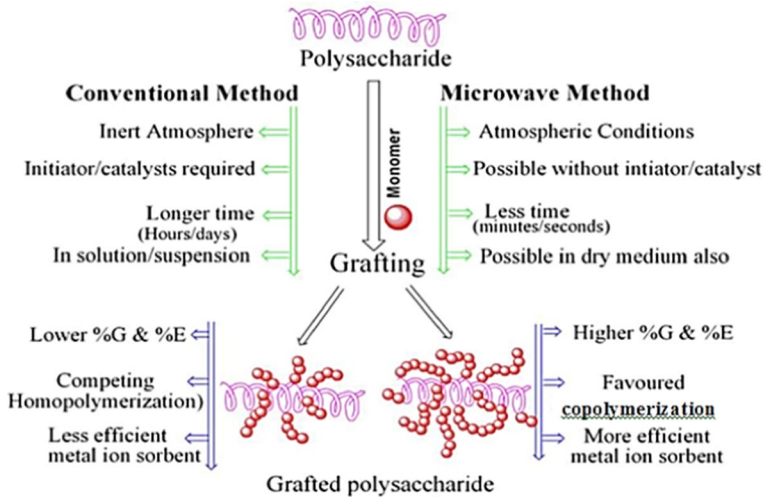
Introduction

Hydrogel is a soft grafted hydrophilic three-dimensional polymeric networks structure that is synthesized from natural polysaccharides or synthetic poly methacrylate esters; it is chemically or physically cross-linked (chemical cross-linkers include bisacrylamide, epichlorohydrin, and glutaraldehyde), and it is an efficient adsorbent for pollutants such as reactive organic dyes in wastewater inside its pores [1]. Sodium acrylate grafted guar gum (GG-g-) and poly acrylamide-g-GG for crystal violet dye removal [2, 3] and GG-g-poly methyl methacrylate for different dyes [4] are some effective hydrogels for removing reactive dyes from wastewater. GG-g-poly (acrylamide)/SiO₂ for acid red dye [5], GG-g-poly (acrylic acid-aniline) for methylene blue (MB) dye, hydrogels of poly (ethylene glycol) acrylamide for AR18 dye, chitosan-g-poly acrylamide for Congo red dye, GG-g graphene for MB dye and chitosan-g-glutaraldehyde for CR dye, and grafted biopolymer for naphthenic acid [6, 7].

Guar gum is a natural plant polymer made up of a linear poly-1, 4-anhydromannose attached to galactose residues at C6 position, a 2:1 mannose/galactose ratio, and an excess of hydroxyl (OH) groups comparable to chitosan [8]. Microwave grafting of monomers on the backbone of polymers improved the mechanical and thermal properties of GG-g-hydrogel [9], and it is the best method for most polysaccharides, such as cellulose and starch, because it uses a water polar solvent that efficiently absorbs microwave radiation, resulting in a large amount of heat energy and, as a result, a high grafting yield [4, 10]. The main advantage of microwave grafting over traditional grafting was shown in Scheme 1 [10].

Low-cost adsorbents made by the traditional grafting approach have some drawbacks: GG Algal biomass, bagasse: horn snail (*Telescopium* sp), mud crab (*Scylla* sp) shells for Cu(II) ions [11, 12]; telescope snail@mangrove crab shell powder for Pb(II) [13]; bagasse-bentonite for Cd(II) [14] and Pb(II), respectively [15], algal biomass waste-bentonite for Pb(II) [16], Archontophoenix *Alexandrae* for (Cu(II), Zn(II), and Ni(II)) [17], and mercapto-silica gel hybrid for Cu (II) and Pb(II). Smart grafted polymers (starch, alginate, chitosan, and lignin are used for: removal of CR dye [19], medication delivery system [5], and different fields of technology such as double-network electrolytes for metal-air batteries [20–23] and dye-sensitized solar cells [24–29]).

AR8 dye removal by photo-degradations [28, 29] and starch-g-poly (*N,N*-dimethyl acrylamide) [30–32] has received little attention. Despite substantial research into the synthesis and characterization of hydrogels made of natural and synthetic polymers, the use of *N, N'*-methylene-bis-acrylamide cross-linker in the synthesis



Scheme 1 compares the properties of traditional and microwave polysaccharide techniques

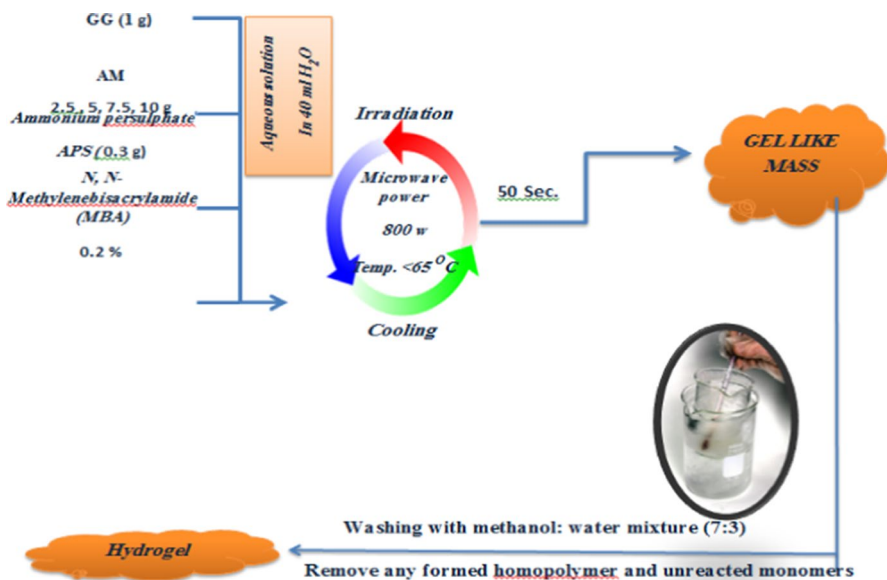
of guar gum-g-acrylamide hydrogels has not been reported yet. Our study is unique in that it intends to synthesize a low-cost, high-efficiency guar gum-g-poly (acrylamide) hydrogel utilizing microwave-aided grafting, as well as test the hydrogel for the removal of anionic acid red 8 (AR8) dye from aqueous solution using a single batch adsorption approach. AR8 dye was chosen for the adsorption study because it is the most carcinogenic hazardous dye found in textile mill and tannery effluents. AR8 is harmful to both the environment and human health since it colors water and reduces dissolved oxygen in wastewater and the textile industry. The microwave-assisted synthesis and assessment of an effective hydrogel for eliminating AR8 dye has yet to be published.

Materials and methods

All of the materials and chemicals utilized in this work are of analytical grade, and they are used exactly as they are without further purification (Supplementary information (SI) section).

Preparation and characterization of guar gum-g-poly (acrylamide) hydrogel

Following acrylamide grafting procedures on polysaccharide [4, 6, 10, 11, 24, 33], one gram GG is swelled in 40 mL distilled water and agitated using a heater with magnetic stirrer. The weights 2.5, 5, 7.5, and 10 g AAM are sequentially dissolved in 10 mL distilled water, added dropwise to the swollen GG solution under continuous vigorous stirring, mixed well, and transferred to the reaction vessel (250 mL conical flask) followed by APS addition. MBA, the necessary amount of cross linker, is added while stirring vigorously. After that, the reaction vessel is placed in an 800 W,



Scheme 2 Microwave production of GG-g-poly AM hydrogel schematic illustration

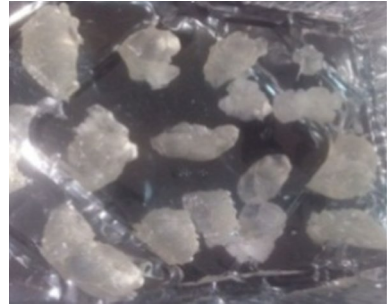
Table 1 The synthesized grades of GG -g-AAM hydrogel

Hydrogel grade	GG		AAM		MBA		APS		Total Weight (g)
	Wt. (g)	%	Wt. (g)	%	Wt. (g)	%	Wt. (g)	%	
1	1	26.26	2.5	65.66	0.008	0.2	0.3	7.88	3.80
2		15.84	5	79.21	0.013	0.2		4.75	6.31
3		11.34	7.5	85.06	0.018	0.2		3.40	8.81
4		8.83	10	88.32	0.023	0.2		2.65	11.32

65 °C microwave oven. To prevent any competitive homopolymerization of GG or AAM, the temperature of the reaction mixture is monitored. After 3 min of irradiation, the microwave irradiation–cooling cycle is repeated until a viscous gel-like mass is formed. Once microwave irradiation process is completed, reaction vessel and its contents were cooled to complete the grafting reaction. The formed hydrogel is extracted using methanol/water mixture (7:3 v/v) to remove any homopolymer and unreacted monomers, washed several times with water, cut into small parts, dried in a hot air-oven at 60 °C till constant weight, and ground. Synthesis process is outlined in Scheme 2, and the composition of various grades of GG -g-PAAM hydrogel is given in Table 1.

Physical cross-linking was improved by heating and chilling the polymer solution due to ionic and hydrogen bonding interactions.

Fig. 1 GG-g-PAM hydrogel photograph (weight ratio: AM/ GG 10:1)



With weight ratios of AAM/guar gum of 2.5:1, 5:1, 7.5:1, and 10:1, the GG-g-AAM hydrogels were successfully synthesized. The hydrogel is translucent, soft, and elastic, with a slippery surface shape, as shown in Fig. 1.

This study’s guar gum-g-acrylamide hydrogel contains physically cross-connected co-polymers by PAAM, is semi-crystalline and mechanically stable, and is made up of microspheres with film-like properties. In this work, described microwave-assisted facile synthesis of acrylamide grafted guar gum hydrogels is simple, repeatable, cost-effective, and easy to handle in large scale as well. Additionally, raw materials are easily available and cheaper.

All characterization methods of analysis and evaluation of the hydrogel adsorption capacity are represented in SI section (Characterization and evaluation of the hydrogel adsorbent).

The average dye absorbance of triplicates is plotted against dye concentration [19], as shown in Fig. 1SI. The linear regression analysis of absorbance versus concentration yielded a good straight line. R^2 0.99 is the correlation coefficient, while the absorptivity coefficient of AR8 dye is 0.0264, which is the slope of the straight line. The residual dye concentration (of known absorbance) is determined through the interpolation of the absorbance data to x -axis.

Table 2 Percent grafting (% G) and grafting efficiency (% GE) of GG-g-PAM hydrogels

Grade	Weight (g)			(% G)	(% GE)
	GG (W_0)	AM (W_2)	GG-g-PAM (W_1)		
GG-g-PAM1	1	2.5	1.59	59	236
GG-g-PAM2	1	5	3.59	259	518
GG-g-PAM3	1	7.5	6.89	589	785
GG-g-PAM4	1	10	9.92	892	892

Results and discussion

According to Scheme 1SI, the preparation procedure for GG-g-PAM hydrogel synthesis is addressed in detail in supplementary information section.

Grafting percentage (%G) and grafting efficiency (%GE) of hydrogel are listed in Table 2.

Grafting is more productive and simple in microwave-assisted reactions due to heterogeneous reaction circumstances (GG immiscible in water), and the heterogeneity of the reaction contents has a substantial impact on grafting yield, which is usually higher than in fully miscible systems [4, 10, 15]. The grafting yield of hydrogel grade 4 in this work (GG-g-AAM4) was 892 percent, which is significantly higher than the published GG-g-poly (acrylonitrile, grafting yield 188 [2].

Characterization of the hydrogel

FT-IR spectra for native GG and AM monomer are shown in Fig. 2. The distinctive vibrational bands at the characteristic wavenumbers were assigned [16].

FTIR vibrational spectral bands are assignment according to wavenumber, $\bar{\nu}$ cm^{-1} —for native GG: a broad band at 3408 cm^{-1} (O–H stretching vibration), 2932 cm^{-1} (C–H stretches of CH_2 group), 1654 cm^{-1} (ring stretches and associated water molecule), 1432 cm^{-1} (Symmetrical deformations of CH_2 group), 1152 and 1092 cm^{-1} (C–OH and primary alcoholic CH_2OH stretching mode). For native acrylamide monomer: 3351 and 3195 cm^{-1} (stretching vibration of the amide functional group (NH_2)), 2813 cm^{-1} (C–H stretches of CH_2 group), 1674 cm^{-1} (stretching vibration of C=O in amide group), 1609 cm^{-1} (C=C stretching vibration), 1430 cm^{-1} (C–N stretching vibration. For GG-g-PAM hydrogel: broad band at

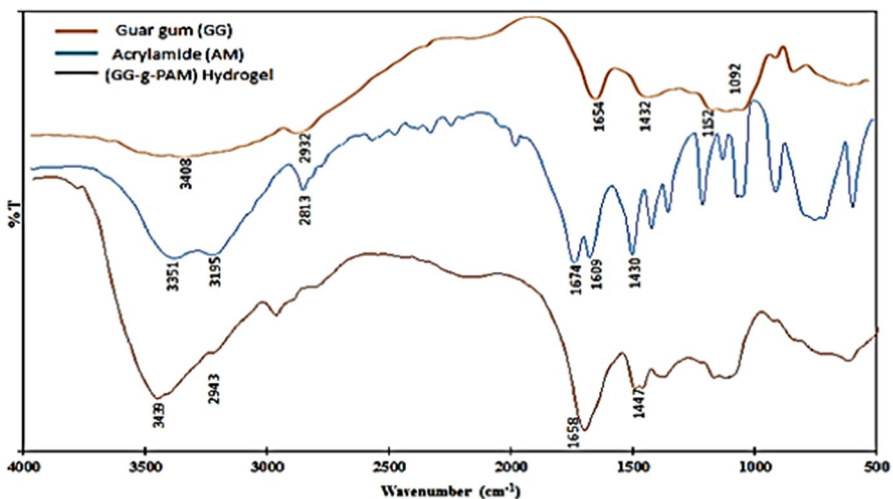


Fig. 2 FTIR spectrum of native GG, AAM, and GG-g-PAM hydrogels

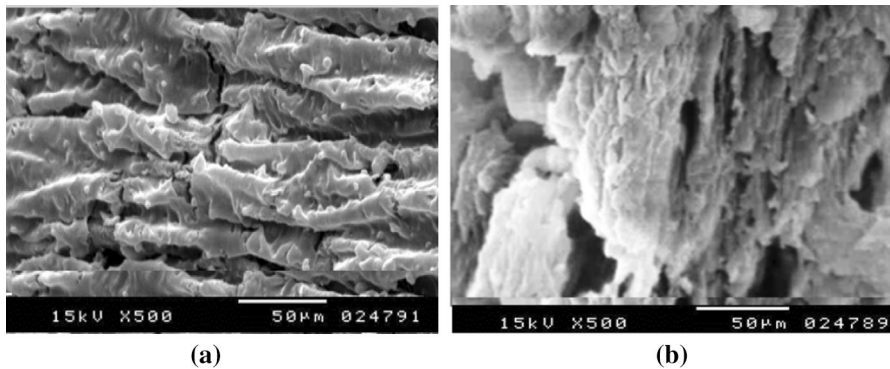


Fig. 3 SEM micrographs of, $\times 500$ magnification: **a** native guar gum polysaccharide and **b** hydrogel at

3439 cm^{-1} (Overlapping of O–H, N–H), 2943 cm^{-1} (C–H stretches of CH_2 group), 1658 cm^{-1} (stretching vibration of C=O in amide group), and 1447 cm^{-1} (C–N stretching vibration). Characteristic vibration band at 1658 cm^{-1} on hydrogel for amide group and disappearance of C=C stretching, vibration band at 1609 cm^{-1} confirmed grafting of AAM on GG backbone [18, 34–38].

SEM micrographs of both GG and hydrogel are shown in Fig. 3a, b. Due to the grafting of AM onto GG backbone chains, the morphological appearance of GG-g-PAM hydrogel compared to native GG sample revealed smoother surface and less roughness than GG surface. The GG polymeric chains become more overlapping, giving the hydrogel a sponge-like structure.

Surface analysis using SEM and FTIR spectra confirmed adsorption of CR dye onto hydrogels pores size of $80\text{ }\mu\text{m}$ masked by dye particles. The strong morphology change of the microstructure of hydrogel (Fig. 3a) than native GG (Fig. 3b) indicated that the hydrogel is chemically and physically cross-linked containing biodegradable and nontoxic guar gum. As previously reported [39], $^1\text{H-NMR}$ spectrum of AAM, GG, and the hydrogel (Fig. 4a–c) confirmed the high grafting percentage of GG by poly AAM. There is a slight proton shift in AAM due to the less number of protons in its molecular structure containing protons in the amide group [17].

The $^1\text{H-NMR}$ spectrum of GG showed the characteristic chemical shift for proton in group and non-equivalent proton shifts in hydroxyl groups. The $^1\text{H-NMR}$ spectra of the hydrogel showed the shift of GG signals toward lower field, since the extensive formed hydrogen bond between H atom and either (N or O) leads to the decrease in the π -electron density on AAM. The shift magnitude is higher with signals due to multiple in the hydrogel that exhibits new signals at chemical shift, the range 3–4 ppm that are assigned to the proton of ($\text{CH}=\text{N}^+-\text{H}$) group of AAM after successful grafting to guar gum. Downfield shift of the signals corresponding to H^+ of GG sugar rings is caused by deshielding effect of positive hole left on these rings after the interaction with AAM [17].

The thermal stability of native GG and hydrogel was clearly exhibited by TGA and DTA thermograms. Figure 5a, b for GG showed a three-stage thermogram: starting from 30 to $175\text{ }^\circ\text{C}$ with 13% weight loss (wt. loss) due to dehydration,

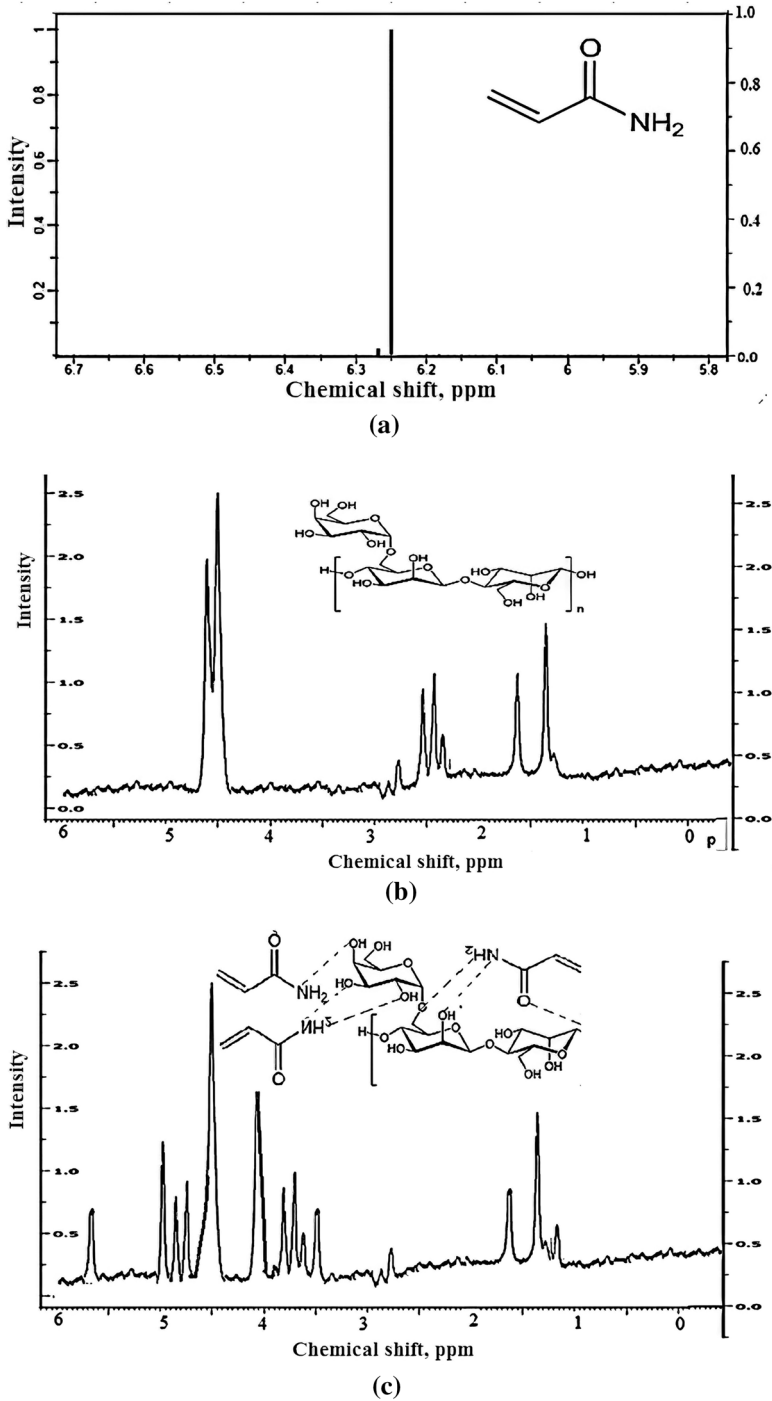


Fig. 4 a $^1\text{H-NMR}$ spectrum of AAM, b $^1\text{H-NMR}$ spectrum of AAM, c $^1\text{H-NMR}$ spectrum of the hydrogel

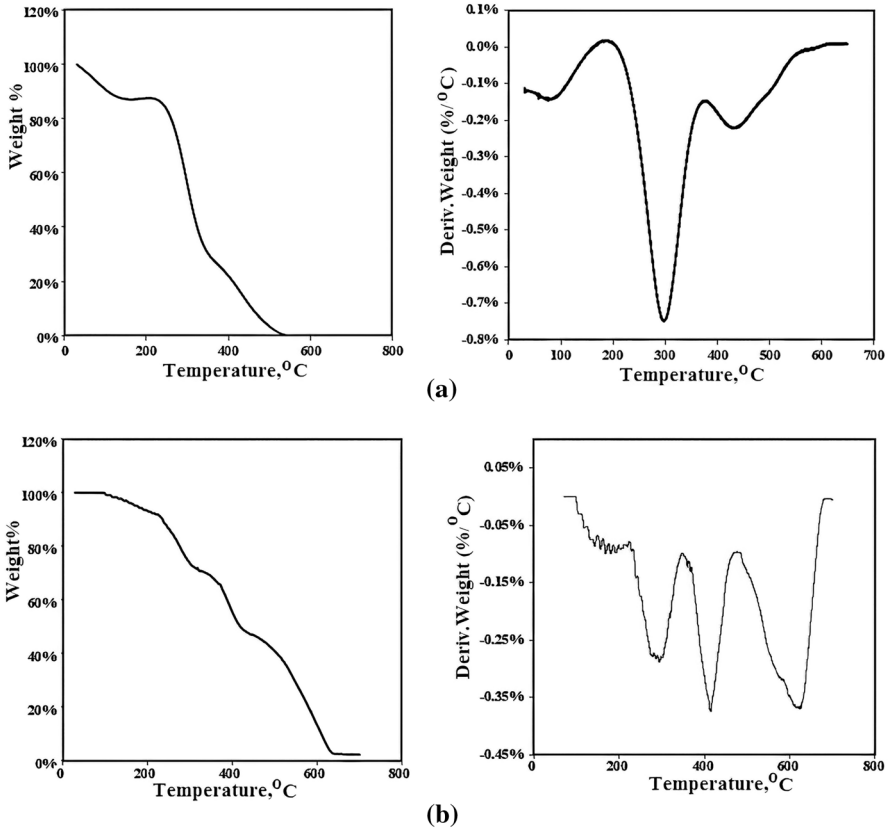


Fig. 5 a TGA and DTG thermograms of GG, b TGA and DTG thermograms of GG-g-PAM hydrogel

60%wt. loss from 175 to 366 °C due to cleavage of galactose and mannopyranose of GG backbone, and 27% wt. loss from 366 to 550 °C due to decomposition of galactose and mannopyranose units. In hydrogel: degradation starts from 100 to 220 °C with 8% wt. loss due to dehydration increasing final temperature of this stage due to difficulty of removing physically absorbed water from hydrogel pores, 23% wt. loss from 220 to 350 °C due to cleavage of galactose and mannopyranose of GG backbone, 24% wt. loss from 350 to 470 °C due to decomposition of galactose and mannopyranose units. 45% wt. loss from 470 to 700 °C is attributed to degradation of PAAM and cross-linked hydrogel. Hydrogel is more

Table 3 Decomposition temperatures of GG and GG-g-PAM hydrogel

Sample	Weight loss (%) at different temperatures				
	150 °C	250 °C	350 °C	450 °C	550 °C
GG	13%	17%	70%	88%	99%
Hydrogel	3%	14%	32%	53%	72%

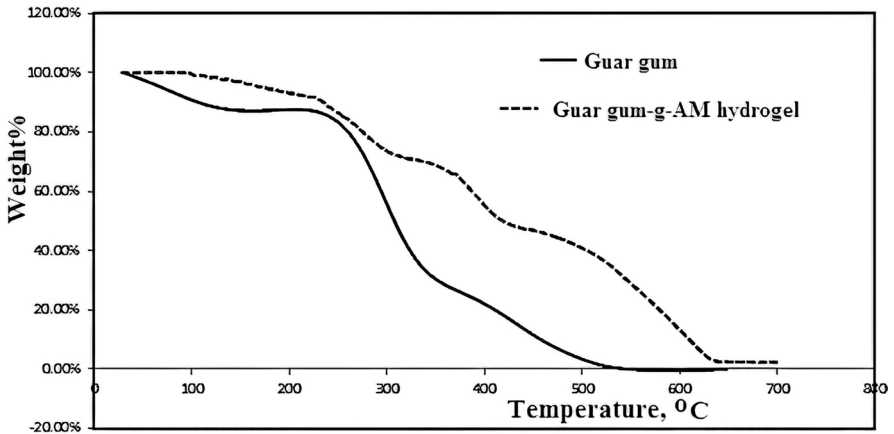


Fig. 6 Comparative TGA thermograms of GG and the hydrogel

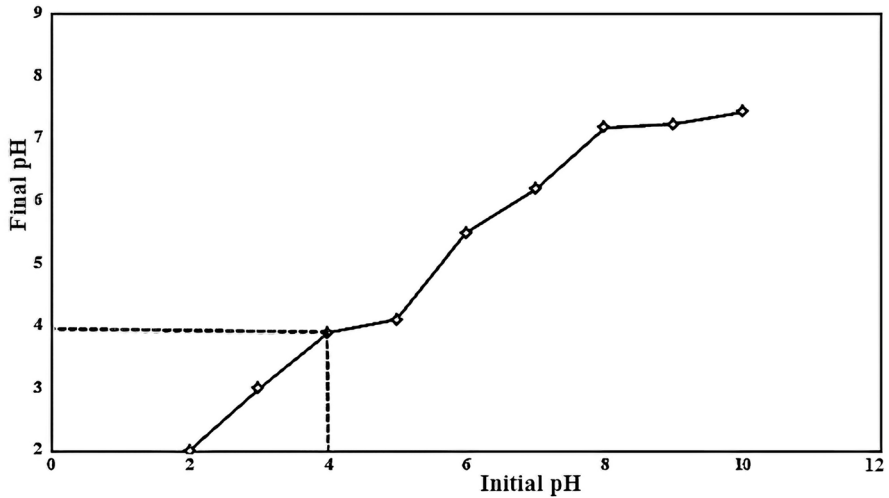


Fig. 7 pH_{pzc} of GG-g-PAM hydrogel by pH drift method

thermally stable than native GG. The percentage wt. loss at different temperature intervals for GG and hydrogel samples is listed in Table 3, and the comparison between TGA of both samples is represented in Fig. 5b.

Comparative TGA thermogram of GG and hydrogel represented showed that the grafting of GG by PAAM enhanced the thermal stability of the hydrogel, Fig. 6.

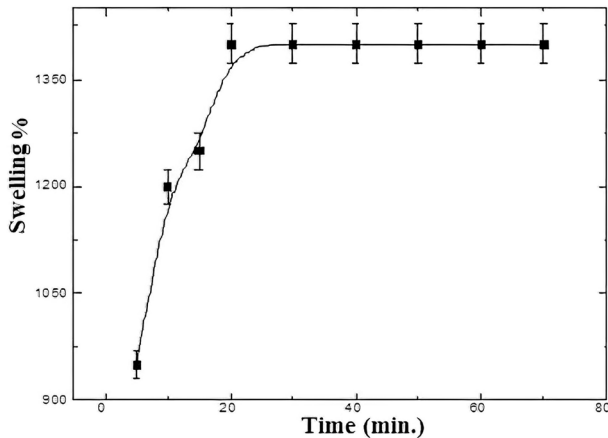


Fig. 8 Swelling ratio (%) of GG-g-PAM hydrogel in deionized water at pH 1

Point of zero charge (PZC) of prepared (GG-g-PAM) hydrogel

Figure 7 shows that pH_{pzc} of hydrogel at pH 4.0. Below pH_{pzc} , hydrogel surface is positively charged favoring adsorption of anionic AR8 dye via electrostatic interaction, while the above pH_{pzc} hydrogel favors the adsorption of cationic dyes [19].

Wastewater contains AR8 dye which is acidic (pH 3.1). Hence, the surface of the hydrogel carries a positive charge at this pH and effectively adsorbs the anionic AR8 dye using its positively charged functional groups.

Swelling of the hydrogel is affected by: immersion time, polymer composition, solvent, specific surface area, percentage of the cross-linker, pore size and hydrogel-hydrophilic groups. Swelling of 0.1 g hydrogel in deionized water via at pH 1 for different time intervals, the obtained data are represented in Fig. 8. The percent of swelling ratio (%SR) initially increased with time till equilibrium at which no further increase in water uptake with time. The %SR was 1360% after 20 min. The swelling of the hydrogel may be due to protonation of: hydroxyl ($-\text{OH}$) groups of GG at low pH and acryl amino groups (CONH_2) of which resulted in electrostatic repulsion between the same charged ions. The observed equilibrium may be due to the full occupation of hydrogel pores which restricted the entry of further water molecules into the pores of the hydrogel [20].

Swelling % varies with time as logistic population growth function, initially the swelling % increased exponentially with time, and then the swelling % reached asymptote after 20 min. The high swelling percentage 1400% of the hydrogel by aqueous solution at pH 1 reflected its high ability to absorb the toxic reactive AR8 from the polluted aqueous solution at 20 min. The high swelling percentage 1400% of the hydrogel by aqueous solution at pH 1 reflected its high ability to absorb the toxic reactive AR8 from the polluted aqueous solution at 20 min. The constant value of % swelling after 20 min. indicated that this time period is the optimum contact time for swelling the hydrogel in the aqueous solution. The prepared super-absorbent hydrogel in our study has swelling percentage (1400%) exceeding that

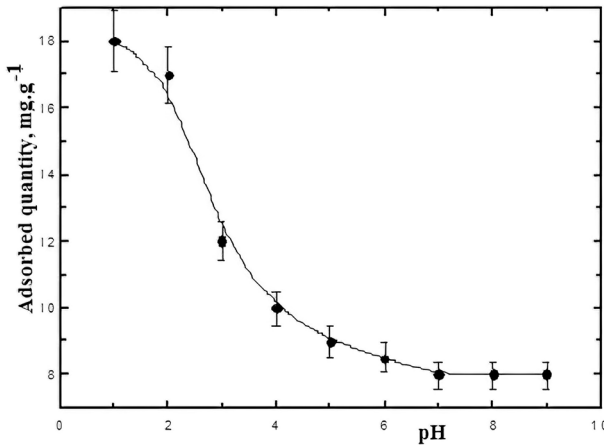


Fig. 9 Effect of pH on adsorbed quantity of AR 8 dye

of chitosan/poly (acrylamide) normal hydrogel (185.3%). The absorption capacity superabsorbent hydrogels is 100 times higher than that of the conventional hydrogel belonged to hydrogels.

Effect of operational parameters on AR8 dye removal

One-way analysis of variance is applied in order to test significant differences in effects among operational adsorption parameters on adsorbed quantity of AR8 dye on hydrogel to test significant differences in effects among these parameters (significance level was set at probability (p) < 0.05). All adsorption data are expressed as average \pm standard deviation.

Figure 9 shows the adsorbed quantity AR8 dye at equilibrium on the hydrogel at the pH range from 1.0 to 9.0. All the adsorption data were carried out in triplicates, and the mean of the average was taken. With a limited standard deviation, the absorbed amount of AR8 dye is decreased from 18 mg.g⁻¹ at pH 1 to 8 mg.g⁻¹ at pH 9.

Where the error bars cross over one other, the effect of pH on the adsorbed quantity of AR8 dye appears to be the same for pH 1 and 2. With pH 5–9, a similar impact is observed. Beyond pH, there appears to be no substantial variation in the percentage of AR8 dye removed. As a result, the real pH effect ranges from 2 to 5.

The average adsorbed quantity is decreased on increasing pH. All trials showed a significant effect of pH ($p < 0.05$).

This reflects the electrostatic adsorption mechanism of anionic AR8 dye on cationic hydrogel. Maximum adsorption capacity of AR8 (q_e) at pH 1.0 is due to available extensive protonated NH_3^+ and OH_2^+ as effective binding sites for AR8 dye. Adsorption capacity (q_e) of AR8 dye dropped from (18 mg.g⁻¹) to (8 mg.g⁻¹) with increasing pH (5–9). This decrease in q_e is because high OH^- concentration deprotonates amino (NH_3^+) and hydroxyl groups (OH_2^+) that attract anionic

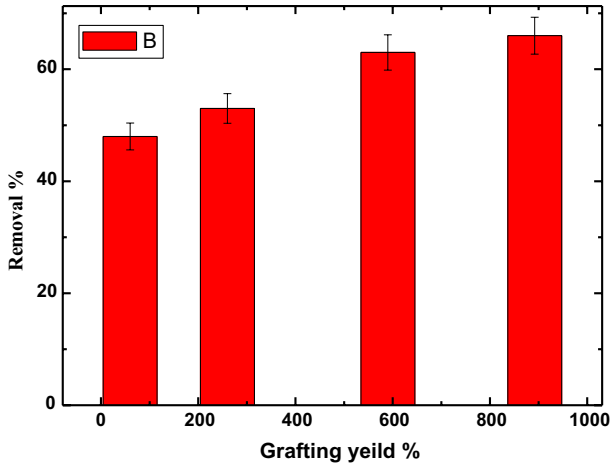


Fig. 10 Effect of (% *G*) of hydrogel on AR8 dye removal (%)

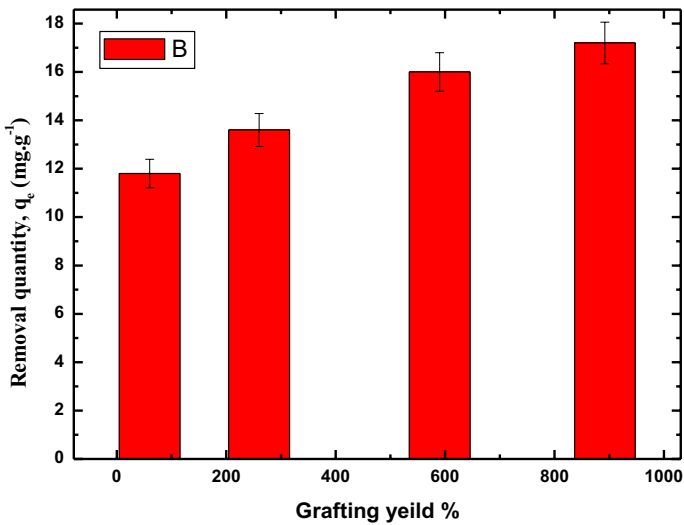


Fig. 11 Effect of (% *G*) of hydrogel on adsorbed quantity of AR8 dye

dye [22]. The effect of % *G* for four hydrogel grades on % removal dye and the adsorbed quantity (mg. g⁻¹) is represented in Figs. 10 and 11. Removal percentage increased from 47 to 66% as % *G* increased from 60 to 892%. Adsorbed amount (mg. g⁻¹) increased from 12 to 17 for the same increase in %*G* due to increasing number of grafted NH₂ functional groups on backbone polymeric chain of GG.

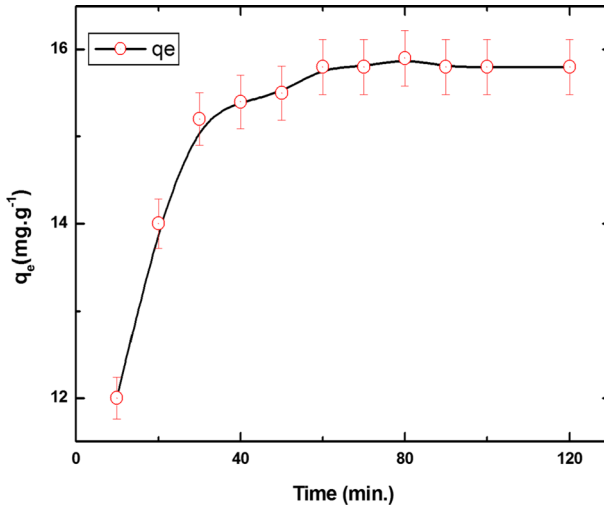


Fig. 12 Effect of contact time on quantity adsorbed (mg. g^{-1}) of AR 8 dye on the hydrogel ($n=3$, $\text{SE} \pm 0.31$)

The variation of removal % and removed quantity, q_e , of AR8 dye (from wastewater through adsorption) showed python frequency histogram where the highest value of these two parameters is achieved at 892% grafting yield of hydrogel.

The effect of contact time on quantity of adsorbed dye is shown in Fig. 12. The adsorbed quantity increased rapidly in first 10 min. (12 mg. g^{-1}) due to the presence of more available vacant sites and increasing the concentration gradient between adsorbate in solution and adsorbate on hydrogel surface, and then increased gradually reaching equilibrium state at 60 min. (16 mg.g^{-1}). Over time, concentration gradient decreases because of dye molecules accumulation in vacant sites, so adsorption rate becomes limited [23].

The optimum contact time for the removal of AR8 is comparable to the removal of the same dye using photodegradation [28] and $\text{Cu}_2\text{O@TiO}_2$ nanocomposite [30]. Also optimum pH (1) for AR8 dye adsorption on hydrogel prepared in this study is consistent to pH of anionic dyes [28, 30].

Up to 40 min of contact time had a significant effect on adsorption ($p < 0.05$). However, increasing the interaction time to 40 min had no effect ($p > 0.05$).

Linear fitting of the adsorption data to the common kinetic models data is represented in Fig. 2SI-4SI. Plot $\log(q_e - q_t)$ against time (t) for pseudo-first-order kinetic model (Fig. 2SI) yields a nonlinear regression relationship (small correlation

Table 4 kinetic parameters of pseudo-second-order model for adsorption of AR8 on hydrogel

$q_{e(\text{exp.})}(\text{mg. g}^{-1})$	Pseudo-second-order kinetic model			
	$k_2(\text{g. mg}^{-1}. \text{min}^{-1})$	$q_e(\text{mg. g}^{-1})$	R^2	(MSE)
16	0.0174	16.72	0.996	0.010

coefficient, R^2 0.4687, and high mean squared error, MSE (0.373), indicating that AR8 dye adsorption on hydrogel does not fit this kinetic model. Plot t/q_e versus time (Fig. 3SI) showed good linear fitting: $1/k_2q_e^2$, $1/q_e$ are intercept and slope of the straight line, respectively (R^2 0.996), indicating that the adsorption kinetics followed pseudo-second-order kinetic [15, 17]. All parameters and corresponding linear regression are listed in Table 4.

The high value of R^2 (0.996) and low value of MSE (0.010) reflect the good linear relation between the adsorption data and time. The adsorption kinetic followed the pseudo-second-order model.

Figure 4SI shows fitting of adsorption data to intraparticle diffusion model. Non-linear relation between qt versus $t^{1/2}$ (R^2 0.81, MSE 0.061) indicates that intraparticle diffusion of dye molecules is not the only rate controlling step for dye adsorption on hydrogel surface. Hence, this model is not suitable for describing adsorption kinetic of dye molecules on surface of hydrogel. Figure 5SI shows that adsorption data not fitted Elovich model kinetic model (R^2 0.892, MSE 0.071). AR8 dye adsorption onto hydrogel is not controlled by chemisorption and ion exchange mechanism. The physisorption of dye molecules is the predominant adsorption mechanism.

Removal % and adsorbed quantity (mg.g^{-1}) using different hydrogel dosage are shown in Fig. 13a, b. The % dye removal on using 0.5 g.L^{-1} hydrogel is 34.0%; with increasing the dosage, it reached a maximum value of 87% at 8.0 g.L^{-1} hydrogel. Using hydrogel dosage above 8.0 g.L^{-1} , % dye removal remains almost constant, indicating that dose of 8.0 g.L^{-1} is sufficient for optimum dye removal. Increasing % dye adsorption with increasing hydrogel dosage in first stage could be due to greater availability of the exchangeable sites of hydrogel. The leveling of removal (%) at a high hydrogel dosage is attributed to the maximum exhaustion of dye upon using 8.0 g.L^{-1} adsorbent dosages. The adsorbed quantity AR8 decreased from 34 to 5.5 mg.g^{-1} with increasing hydrogel dose from 0.5 to 8.0 g.L^{-1} .

High removal percentage, 87% AR8 dye by the hydrogel is much higher than many values [19, 28, 30, 31, and 39]. The adsorbed amount of the dye at equilibrium

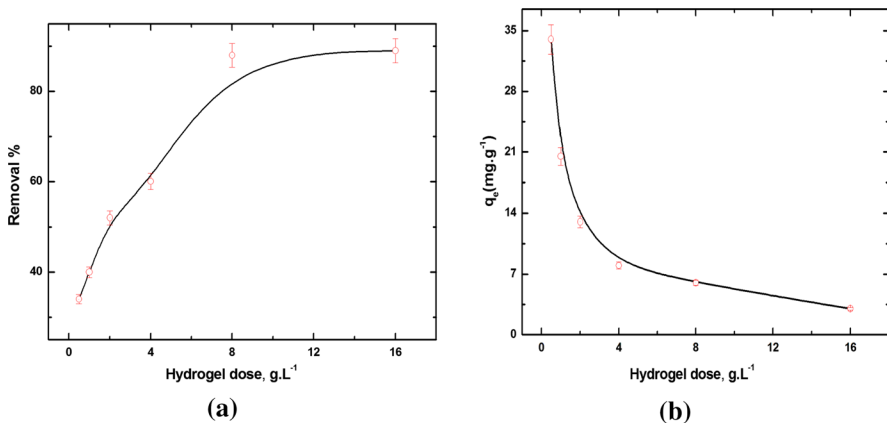


Fig. 13 Effect of GG-g-PAM hydrogel dose on: **a** % dye removal ($n=3$, $\text{SE} \pm 0.40$), **b** adsorption capacity of hydrogel ($n=3$, $\text{SE} \pm 0.29$)

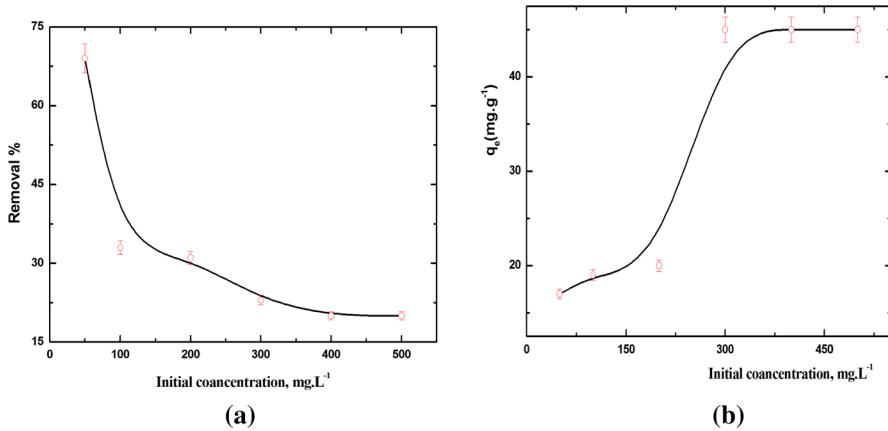


Fig. 14 Effect of initial dye concentration on: **a** Removal% ($n=3$, $SE \pm 0.47$), **b** adsorption capacity of hydrogel ($n=3$, $SE \pm 0.53$)

decreased with increasing the dosage of the hydrogel. Hydrogel dose has a significant effect below 8 mg.L^{-1} ($p < 0.05$), but above this value, the elimination percentage becomes limited ($p > 0.05$).

Figure 14a, b shows that percentage of AR8 dye removal dropped from 68 to 20% on increasing its initial concentration from 50 to 500 mg.L^{-1} . This finding is due to the fact that at low dye concentrations there are sufficient unoccupied active sites on hydrogel for attraction of more dye molecules, whereas at higher dye concentrations there are a limited number of un-occupied active sites which causes competition between dye molecules for adsorption; consequently, the removal % dye decreases [25].

When the original dye concentration (C_i) is increased to 300 mg.L^{-1} , the removal efficiency drops considerably. ($p < 0.05$). The removal % does not change significantly with increasing C_i above this optimal C_i ($p > 0.05$).

Figure 14 b shows that the adsorbed quantity (mg.g^{-1}) of AR8 dye increased from 17 to 44 mg.g^{-1} with increasing AR8 dye concentration from 50 to 300 mg.L^{-1} and becomes constant after this concentration. This is because at higher dye concentration there is high driving force to overcome mass transfer resistance of AR8 dye between solid and aqueous phases and accelerating diffusion of AR8 dye molecules into adsorbent, so the quantity adsorbed (mg.g^{-1}) increased with increasing initial dye concentration [26].

Figure 15 displays temperature effect on adsorption capacity (q_e) of AR8 dye on the hydrogel. Adsorbed quantity of AR8 dye is decreased on elevating the temperature from 20 to 50 °C. The value of q_e decreased from 17 to 13 as increasing dye solubility and its solvation by water retard adsorption, hydrogel-dye interactions decline due to increasing kinetic energy and the mobility of dye molecules at high temperature [27].

The optimum low temperature 20 °C for the removal of AR8 dye by the GG-g-AAm hydrogel reflects exothermic strong bond formation between the hydrogel and

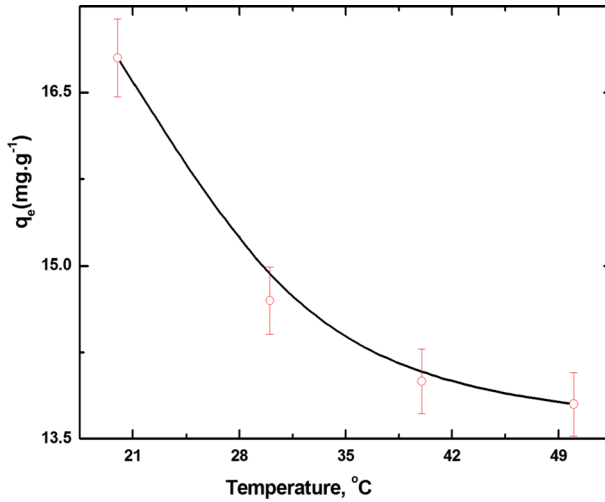


Fig. 15 Temperature effect on adsorption capacity of hydrogel ($n=3$, $SE\pm 0.71$)

the dye molecules. The exothermic nature of adsorption of AR8 dye on the hydrogel led to heat energy saving in contrast to endothermic adsorption of ionic dyes on various adsorbents [19, 28, 30, 31, 39].

Crosstab statistical analysis of all values adsorbed quantity at each adsorption parameter showed small variance of the values of q_e reflecting accurate determination of this parameter and the probability (p) < 0.05 for all tested parameters pH, contact time, agitation speed, and initial dye concentration temperature are all have significant effect on the values of q_e .

The statistical analysis concluded that increasing contact time, hydrogel dosage, and starting dye concentration over 40 min, 16 mg.L⁻¹, 300 mg.L⁻¹ had no influence on the proportion of dye that was removed (probability P 0.05). While low values of all of these parameters had a significant effect on removal efficiency (P 0.05), high values had no effect.

The calculated thermodynamics parameters of adsorption of AR8 dye are collected in Table 5. Standard Gibbs free energy ($\Delta G^{\circ}_{ads.}$), standard enthalpy ($\Delta H^{\circ}_{ads.}$), and standard entropy ($\Delta S^{\circ}_{ads.}$) were calculated using equations (22–24, SI). Using

Table 5 Thermodynamic data for AR8 dye adsorption on hydrogel at different temperatures

Temperature (°K)	$\Delta G^{\circ}_{ads.}$ (kJ.mol ⁻¹)	$\Delta H^{\circ}_{ads.}$ (kJ.mol ⁻¹)	$\Delta S^{\circ}_{ads.}$ (J.mol ⁻¹ .K ⁻¹)
293	-1.61	-15.17	-46.76
303	-0.81		
313	-0.42		
323	-0.21		

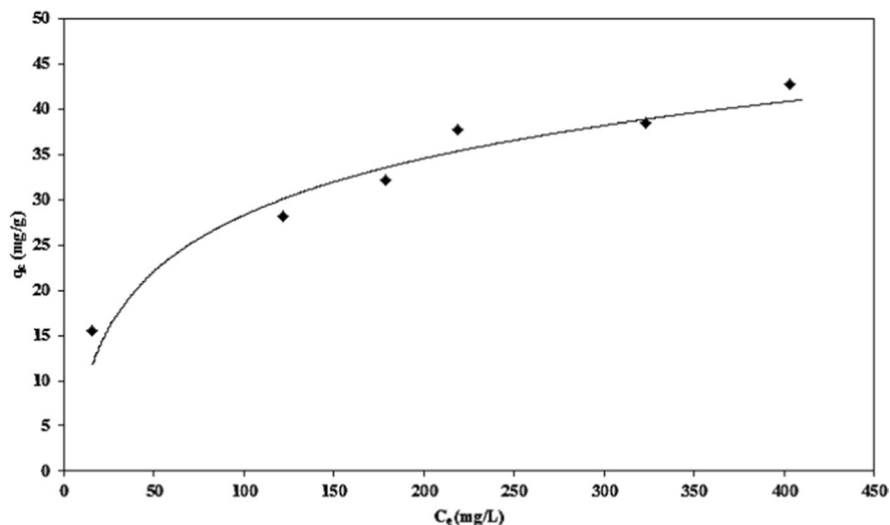


Fig. 16 Adsorption isotherm of AR8 dye on GG-g-PAM hydrogel

Table 6 Langmuir separation factor (R_L) at different initial AR8 dye concentrations

Initial AR8 concentration (mg. L ⁻¹)	50	100	200	300	400	500
R_L	0.5542	0.3846	0.2940	0.2380	0.2000	0.1724

adsorption data at different temperatures, ΔH°_{ads} , and ΔS°_{ads} , are calculated by plot $\ln K_d$ versus $1/T$ using linear regression method (Fig. 6 SI).

The negative values ΔG°_{ads} , confirmed feasible and spontaneous adsorption at the described experimental conditions. The negativity of ΔG°_{ads} , decreased on rising temperature indicates that adsorption process is less favored and less spontaneous at high temperatures [29]. The values of ΔG°_{ads} , are less than $-20 \text{ kJ}\cdot\text{mol}^{-1}$ signifying predominance of physisorption [29]. Negative ΔH°_{ads} , indicating exothermic adsorption and its low value indicated physisorption. The low ΔH° values counsel that weak energies are concerned within AR8 dye adsorption on the hydrogel. Typically, ΔH°_{ads} , for physisorption ranges from -4 to $-40 \text{ kJ}\cdot\text{mol}^{-1}$ and from -40 to $-800 \text{ kJ}\cdot\text{mol}^{-1}$ for chemisorption. Negative ΔS°_{ads} , reflects hydrogel affinity to the dye molecules and suggests strong interaction giving more ordered adsorption system [28].

Figure 16 shows the S-shaped adsorption isotherm of AR8 dye at 20°C , equilibrium concentration and different initial concentrations of AR8 dye.

Up to the initial dye concentration $400 \text{ mg}\cdot\text{L}^{-1}$, the residual dye concentration is limited to 40 mg/g hydrogel. This adsorption mechanism followed Type I adsorption isotherm according to IUPAC classification indicating strong interaction between dye molecules and active sites of the hydrogel.

Hydrogel adsorption capacity for AR8 dye was estimated by fitting adsorption data to Langmuir and Freundlich adsorption isotherms (Figs. 7SI, 8SI). Langmuir

Table 7 Adsorption parameters obtained from Freundlich and Langmuir equations

	Q_o (mg.g ⁻¹)	K_L (L. mg ⁻¹)	R^2
Langmuir parameter	54.054	88	0.951
	$1/n$	K_f (mg. g ⁻¹), (L. mg ⁻¹)	R^2
Freundlich parameter	0.334	203	0.963

plot $\frac{C_e}{q_e}$ versus C_e (7SI) showed good linear fit straight line (slope equals $1/Q_o$, and intercept equals $1/K_L Q_o$). Langmuir constants for adsorption of AR8 onto hydrogel are Q_o (maximum adsorption capacity) 54.054 mg. g⁻¹, K_L (Langmuir constant 8.8×10^{-3} L. mg⁻¹, R^2 0.951. To describe AR8 adsorption, a dimensionless separation factor or equilibrium parameter (R_L) is considered: $R_L > 1$, $0 < R_L < 1$, $= 0$ for unfavorable, favorable and irreversible adsorption, respectively (Table 6).

Values of R_L range from 0.5542 to 0.1724 indicating favorable adsorption of AR8 onto hydrogel surface.

Freundlich plot $\log(q_e)$ versus ($\log C_e$), Fig. 8SI gives good straight line (slope = $(1/n)$, intercept = $(\log K_f)$. Adsorption parameters collected in Table 7.

K_f 203 mg.g⁻¹ or L. mg⁻¹), $1/n$ 0.334, R^2 0.963. Langmuir adsorption isotherm model fitted well with experimental results compared to Freundlich equation based on correlation coefficient (R^2). Hydrogel surface is majorly made up of homogeneous adsorption sites and less heterogeneous sorption sites. Maximum adsorption capacity, Q_o , 54.054 mg.g⁻¹ is almost closer to experimental maximum capacity (44 mg.g⁻¹). This value of maximum adsorption capacity is in a good agreement of hydrogel of poly (acrylic acid)-g-starch 41.7.0 mg.g⁻¹ for methylene blue (MB) dye

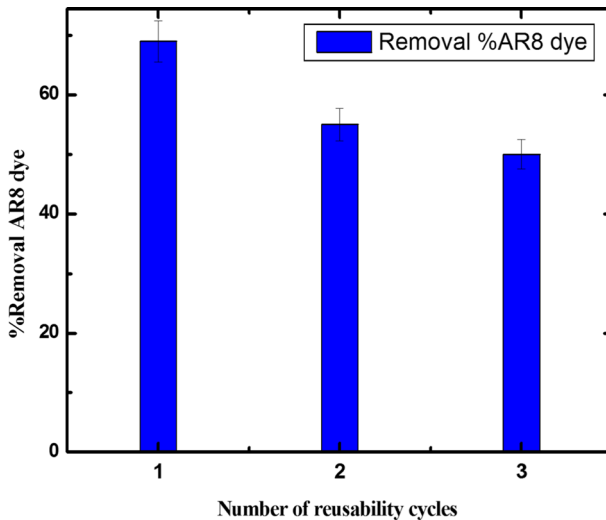


Fig. 17 Reusability of GG-g-PAM hydrogel for adsorption of AR8 dye ($n=3$, $SE \pm 0.76$)

[31]. The adsorption mechanism of AR8 dye by GG-g-PAM hydrogel is depicted in SI.

Reusability study (adsorption–desorption cycle)

Hydrogel reusability is examined to determine its feasibility for industrial application. The dye adsorbed on GG-g-PAM hydrogel was effectively recycled using 1.0 M NaOH solutions because the screening effect of OH^- on adsorbent surface greatly weakened the electrostatic interactions between the hydrogel and dye molecules. Figure 17 proves that hydrogel still had a good adsorption capacity removal percentage of the dye still exceeding 50% for three consecutive cycles (adsorption–desorption cycles). The results confirmed that the hydrogel is mechanically stable and can be applied as a reusable adsorbent for pollutants dyes in the field of industrial wastewater treatment. Further increase in the reuse cycles beyond three cycles decreased the mechanical properties of the adsorbent in which the hydrogel network started to disintegrate.

Adsorption mechanism for removal of reactive dyes by large surface area-adsorbent hydrogel involved physisorption through electrostatic interaction between dye molecules and the functional groups on the hydrogel interaction. The decrease in the removal percentage of the dye at cycles 2 and 3 suggested the contribution of chemisorption involve chemical bond formations that are difficulty broken in 1.0 M NaOH.

Strong change of the microstructure of the hydrogel and the red color of the dye after adsorption suggested the contribution of the chemisorption mechanism with the physisorption mechanism, and the negatively charged AR8 dye electrostatically attracted to positively charged functional groups in the surface of the hydrogel.

Figure 18 confirms the efficient adsorption of AR8 dye on the hydrogel with respect to the color change of the dye and microstructure of the hydrogel.

Before adsorption, AR8 dye in contact to the hydrogel adsorbent at the optimum conditions has dark red color, after adsorption the color of AR8 becomes very faint pink due to efficient incorporation of the dye molecules into the pores of the hydrogel. The relatively smooth surface morphology becomes very coarse after adsorption and the entrapment of the dye molecules into the pores of the hydrogel. Grafted acrylamide onto GG increased the function groups for

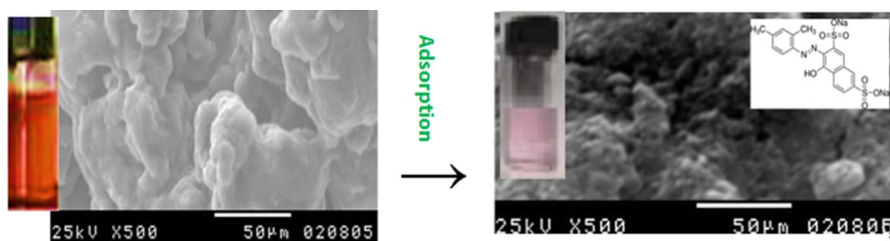


Fig. 18 Change of dye-color and hydrogel-microstructure after adsorption

chelation of AR8 dye. Removal efficiency was higher that reached 70% at 5th cycle of adsorption–desorption.

The work carried out in this study is reproducible, and hydrogel can be prepared in commercial scale for benefits in all society for wastewater treatment. The biodegradability, low cost and sustainable natural guar gum (GG) polymer make it is favored to formulate GG-AAM hydrogel as an efficient alternative biodegradable adsorbent for a sustainable system of wastewater treatment. Quite high costs are required for synthesis adsorbents such as activated carbon which requires very high temperature for pyrolysis of organic matter from plants residue, and anfunctionalized silica gel requires very high cost chemical reagent. It is possible to formulate guar gum-AAM hydrogel using microwave-assisted method in a large commercial scale to use guar gum-g-poly (acrylamide) hydrogel as efficient adsorbent for removal of dyes on a higher scale in companies of wastewater treatments, such as sewage-sludge treatment plants in various industry or society. Hence, Table 8 represents the simplified techno-economics costs of using guar gum-g-poly (acrylamide) hydrogel as adsorbent for removal of dyes according to the price of chemicals in the international Co. for chemical products, 2021.

The adsorbent hydrogel prepared for dye removal from wastewater include is cost, and dye adsorption on hydrogel is safe to the environment causing no toxic products. Dye removal from wastewater by using this hydrogel is facile, feasible, simple, rapid and efficient [2].

The most efficient hydrogel is grade 4 has the chemical composition and costs as represented in Table 8.

The weights of the chemical constituents required for the preparation of the hydrogel are all minor quantities.

Conclusion

In this study, a hydrogel was prepared by grafting acrylamide (AM) onto GG polymeric chains in the presence of APS initiator and MBA cross-linker using microwave-assisted method. The efficient grafting reaction as strongly confirmed by FTIR spectroscopy (the characteristic absorption at 1658 cm^{-1} in the GG-g-AAM hydrogel confirming the amide group of AAM and the disappearance of stretching vibration of C=C band of AAM at 1609 cm^{-1} ., The SEM micrographs confirmed the change in surface morphology of GG-g-PAM hydrogel against native GG. The maximum dye removal (66%) percent was attained at percentage of grafting (892%).

Table 8 Economic study for formulation of guar gum-acrylamide hydrogel adsorbent

Item	Guar gum 4129–250	Acrylamide	<i>N, N</i> -Methylen- ebisacrylamide	Ammonium persulfate	SHARPMi- crowave Solo 20 L
Weight (g)	1.0	10	0.0226	0.3	800 Watt
Unit price	\$1.0	\$210.6	\$280.1	\$0.72–\$3.84	\$16 dollars

The percentage of dye removal on using hydrogel dosage of 0.5 g. L⁻¹ is 34%. This percent increased by increasing the hydrogel dosage and reached 87% at 8.0 g. L⁻¹ hydrogel dose. The adsorption data linearly fitted with Langmuir adsorption model (maximum adsorption capacity of 54.054 mg. g⁻¹), and the adsorption followed pseudo-second-order kinetics assumes that valance forces through electrons transfer between the dye molecules and the hydrogel are involved in adsorption. The adsorbed quantity (q_e) decreased with rising the temperature, and the maximum adsorption was obtained at 20 °C indicating that dye adsorption is exothermic in nature. This finding is confirmed from the negative value of ΔH_{ads} . The spontaneity of dye adsorption on the hydrogel is confirmed from the negative value of ΔG_{ads} . The hydrogel is an economical, non-toxic, efficient, safe superabsorbent with high absorption capacity for the wastewater treatment from the acidic dyes.

Supplementary Information The online version contains supplementary material available at <https://doi.org/10.1007/s00289-022-04254-7>.

Funding Open access funding provided by The Science, Technology & Innovation Funding Authority (STDF) in cooperation with The Egyptian Knowledge Bank (EKB). Funding was provided by Alexandria University (Grant No. 234).

Open Access This article is licensed under a Creative Commons Attribution 4.0 International License, which permits use, sharing, adaptation, distribution and reproduction in any medium or format, as long as you give appropriate credit to the original author(s) and the source, provide a link to the Creative Commons licence, and indicate if changes were made. The images or other third party material in this article are included in the article's Creative Commons licence, unless indicated otherwise in a credit line to the material. If material is not included in the article's Creative Commons licence and your intended use is not permitted by statutory regulation or exceeds the permitted use, you will need to obtain permission directly from the copyright holder. To view a copy of this licence, visit <http://creativecommons.org/licenses/by/4.0/>.

References

1. Krishnappa PB, Badalamoole V (2019) Karaya gum-graft-poly (2-(dimethylamino) ethyl methacrylate) gel: an efficient adsorbent for removal of ionic dyes from water. *Int J Biol Macromol* 122:997–1007
2. Singha NR, Dutta A, Mahapatra M, Karmakar M, Mondal H, Chattopadhyay PK, Maiti DK (2018) Guar gum-grafted terpolymer hydrogels for ligand-selective individual and synergistic adsorption: effect of comonomer composition. *ACS Omega* 3(1):472–494
3. Qureshi MA, Nishat N, Jadoun S, Ansari MZ (2020) Polysaccharide based superabsorbent hydrogels and their methods of synthesis: a review. *Carbohydr Polym Technol Appl* 1:100014
4. Mittal H, Kumar V, Alhassan SM, Ray SS (2018) Modification of gum ghatti via grafting with acrylamide and analysis of its flocculation, adsorption, and biodegradation properties. *Int J Biol Macromol* 114:283–294
5. Maijan P, Amornpitoksuk P, Chantarak S (2020) Synthesis and characterization of poly (vinyl alcohol-g-acrylamide)/SiO₂@ ZnO photocatalytic hydrogel composite for removal and degradation of methylene blue. *Polymer* 203:122771
6. Pakdel PM, Peighambaroust SJ (2018) Review on recent progress in chitosan-based hydrogels for wastewater treatment application. *Carbohydr Polym* 201:264–279
7. Udoetok IA (2018) Modified Biopolymer Sorbents for the Uptake of Naphthenic Acid Fraction Components (NAFCs) from Aqueous Solutions (Doctoral dissertation, University of Saskatchewan)

8. Fetouh HA, Hefnawy A, Attia AM, Ali E (2020) Facile and low-cost green synthesis of eco-friendly chitosan-silver nanocomposite as novel and promising corrosion inhibitor for mild steel in chilled water circuits. *J Mol Liq* 319:114355
9. Mohammadinejad R, Maleki H, Larrañeta E, Fajardo AR, Nik AB, Shavandi A, Sheikhi A, Ghorbanpour M, Farokhi M, Govindh P, Cabane E (2019) Status and future scope of plant-based green hydrogels in biomedical engineering. *Appl Mater Today* 16:213–246
10. Chami S, Joly N, Bocchetta P, Martin P, Aliouche D (2021) Polyacrylamide grafted xanthan: microwave-assisted synthesis and rheological behavior for polymer flooding. *Polymers* 13(9):1484
11. Abdel-Halim ES, Al-Deyab SS (2011) Hydrogel from crosslinked polyacrylamide/guar gum graft copolymer for sorption of hexavalent chromium ion. *Carbohydr Polym* 86(3):1306–1312
12. Darmokoesoemo H, Setianingsih FR, Putranto TWLC, Kusuma HS (2016) Horn snail (*Telescopium sp*) and mud crab (*Scylla sp*) shells powder as low cost adsorbents for removal of Cu²⁺ from synthetic wastewater. *Rasayan J Chem* 9(4):550–555
13. Darmokoesoemo H, Magdhalena PT, Kusuma HS (2016) Telescope snail (*Telescopium sp*) and Mangrove crab (*Scylla sp*) as adsorbent for the removal of Pb²⁺ from aqueous solutions. *Rasayan J Chem* 9(4):680–685
14. Kuncoro EP, Isnadina DRM, Darmokoesoemo H, Dzembrahmatiny F, Kusuma HS (2018) Characterization and isotherm data for adsorption of Cd²⁺ from aqueous solution by adsorbent from mixture of bagasse-bentonite. *Data Brief* 16:354–360
15. Kuncoro EP, Isnadina DRM, Darmokoesoemo H, Fauziah OR, Kusuma HS (2018) Characterization, kinetic, and isotherm data for adsorption of Pb²⁺ from aqueous solution by adsorbent from mixture of bagasse-bentonite. *Data Brief* 16:622–629
16. Kuncoro EP, Soedarti T, Putranto TWC, Darmokoesoemo H, Abadi NR, Kusuma HS (2018) Characterization of a mixture of algae waste-bentonite used as adsorbent for the removal of Pb²⁺ from aqueous solution. *Data Brief* 16:908–913
17. Taha AA, Shaban SM, Fetouh HA, Taha ST, Sabet VM, Kim DH (2021) Synthesis and evaluation of nonionic surfactants based on dimethylaminoethylamine: Electrochemical investigation and theoretical modeling as inhibitors during electropolishing in-ortho-phosphoric acid. *J Mol Liq* 328:115421
18. Naat JN, Neolaka YA, Lapailaka T, Tj RT, Sabarudin A, Darmokoesoemo H, Kusuma HS (2021) Adsorption of Cu (II) and Pb (II) using silica@ mercapto (hs@ m) hybrid adsorbent synthesized from silica of Takari sand: optimization of parameters and kinetics. *Rasayan J Chem* 14(1):550–560
19. Dragan ES, Apopei DF (2011) Synthesis and swelling behavior of pH-sensitive semi-interpenetrating polymer network composite hydrogels based on native and modified potatoes starch as potential sorbent for cationic dyes. *Chem Eng J* 178:252–263
20. Zhang Y, Qin H, Alfred M, Ke H, Cai Y, Wang Q, Huang F, Liu B, Lv P, Wei Q (2021) Reaction modifier system enable double-network hydrogel electrolyte for flexible zinc-air batteries with tolerance to extreme cold conditions. *Energy Storage Mater* 42:88–96
21. Rahman NA, Hanifah SA, Mobarak NN, Ahmad A, Ludin NA, Bella F, Suait MS (2021) Chitosan as a paradigm for biopolymer electrolytes in solid-state dye-sensitized solar cells. *Polymer* 230:124092
22. Galliano S, Bella F, Bonomo M, Giordano F, Grätzel M, Viscardi G, Hagfeldt A, Gerbaldi C, Barolo C (2021) Xanthan-based hydrogel for stable and efficient quasi-solid truly aqueous dye-sensitized solar cell with cobalt mediator. *Solar Rrl*. <https://doi.org/10.1002/solr.202000823>
23. Bella F, Porcarelli L, Mantione D, Gerbaldi C, Barolo C, Grätzel M, Mecerreyes D (2020) A water-based and metal-free dye solar cell exceeding 7% efficiency using a cationic poly (3, 4-ethylenedioxythiophene) derivative. *Chem Sci* 11(6):1485–1493
24. Xu P, Wang C, Zhao B, Zhou Y, Cheng H (2021) A high-strength and ultra-stable halloysite nanotubes-crosslinked polyacrylamide hydrogel electrolyte for flexible zinc-ion batteries. *J Power Sources* 506:230196
25. de Haro JC, Tatsi E, Fagiolaro L, Bonomo M, Barolo C, Turri S, Bella F, Griffini G (2021) Lignin-based polymer electrolyte membranes for sustainable aqueous dye-sensitized solar cells. *ACS Sustain Chem Eng*. <https://doi.org/10.1021/acssuschemeng.1c01882>
26. Piana G, Ricciardi M, Bella F, Cucciniello R, Proto A, Gerbaldi C (2020) Poly (glycidyl ether) s recycling from industrial waste and feasibility study of reuse as electrolytes in sodium-based batteries. *Chem Eng J* 382:122934

27. Radzir NNM, Hanifah SA, Ahmad A, Hassan NH, Bella F (2015) Effect of lithium bis (trifluoromethylsulfonyl) imide salt-doped UV-cured glycidyl methacrylate. *J Solid State Electrochem* 19(10):3079–3085
28. Bento AC, Emídio ES, Hammer P, Nogueira RF (2019) Degradation of acid red 8 dye using photofenton reaction mediated by titanium modified catalysts. *J Braz Chem Soc* 30:2170–2181
29. Sadik WA, El-Demerdash AGM, Nashed AW, Mostafa AA, Hamad HA (2019) Highly efficient photocatalytic performance of Cu₂O@ TiO₂ nanocomposite: influence of various inorganic oxidants and inorganic anions. *J Market Res* 8(6):5405–5414
30. Sadik WAA, El-Demerdash AGM, Abbas R, Gabre HA (2020) Fast synthesis of an eco-friendly starch-grafted poly (N, N-dimethyl acrylamide) hydrogel for the removal of Acid Red 8 dye from aqueous solutions. *Polym Bull* 77(8):4445–4468
31. Singh R, Pal D, Mathur A, Singh A, Krishnan MA, Chattopadhyay S (2019) An efficient pH sensitive hydrogel, with biocompatibility and high reusability for removal of methylene blue dye from aqueous solution. *React Funct Polym* 144:104346
32. Iqbal DN, Shafiq S, Khan SM, Ibrahim SM, Abubshait SA, Nazir A, Abbas M, Iqbal M (2020) Novel chitosan/guar gum/PVA hydrogel: preparation, characterization and antimicrobial activity evaluation. *Int J Biol Macromol* 164:499–509
33. Neolaka YA, Supriyanto G, Kusuma HS (2018) Adsorption performance of Cr (VI)-imprinted poly (4-VP-co-MMA) supported on activated Indonesia (Ende-Flores) natural zeolite structure for Cr (VI) removal from aqueous solution. *J Environ Chem Eng* 6(2):3436–3443
34. Neolaka YA, Lawa Y, Naat JN, Riwu AAP, Darmokoesoemo H, Supriyanto G, Holdsworth CI, Amenaghawon AN, Kusuma HS (2020) A Cr (VI)-imprinted-poly (4-VP-co-EGDMA) sorbent prepared using precipitation polymerization and its application for selective adsorptive removal and solid phase extraction of Cr (VI) ions from electroplating industrial wastewater. *React Funct Polym* 147:104451
35. Neolaka YA, Lawa Y, Naat JN, Riwu AA, Iqbal M, Darmokoesoemo H, Kusuma HS (2020) The adsorption of Cr (VI) from water samples using graphene oxide-magnetic (GO-Fe₃O₄) synthesized from natural cellulose-based graphite (kusambi wood or Schleicheria oleosa): study of kinetics, isotherms and thermodynamics. *J Market Res* 9(3):6544–6556
36. Budiana IGMN, Jasman J, Neolaka YA, Riwu AA, Elmsellem H, Darmokoesoemo H, Kusuma HS (2021) Synthesis, characterization and application of cinnamoyl C-phenylcalix [4] resorcinarene (CCPCR) for removal of Cr (III) ion from the aquatic environment. *J Mol Liq* 324:114776
37. Neolaka YA, Lawa Y, Naat J, Riwu AA, Lindu YE, Darmokoesoemo H, Widyaningrum BA, Iqbal M, Kusuma HS (2021) Evaluation of magnetic material IIP@ GO-Fe₃O₄ based on Kesambi wood (Schleicheria oleosa) as a potential adsorbent for the removal of Cr (VI) from aqueous solutions. *React Funct Polym* 166:105000
38. Aigbe UO, Ukhurebor KE, Onyancha RB, Osibote OA, Darmokoesoemo H, Kusuma HS (2021) Fly ash-based adsorbent for adsorption of heavy metals and dyes from aqueous solution: a review. *J Mater Res Technol*. <https://doi.org/10.1016/j.jmrt.2021.07.140>
39. Shekh MI, Amirian J, Stadler FJ, Du B, Zhu Y (2020) Oxidized chitosan modified electrospun scaffolds for controllable release of acyclovir. *Int J Biol Macromol* 151:787–796

Publisher's Note Springer Nature remains neutral with regard to jurisdictional claims in published maps and institutional affiliations.

Authors and Affiliations

Mervette El Batouti¹  · Wagih Sadik² · Abdel Ghaffar Eldemerdash² · Esra Hanafy² · Howida Abouel Fetouh¹

✉ Howida Abouel Fetouh
howida_fetouh@alexu.edu.eg

Mervette El Batouti
mervetteb@yahoo.com

- ¹ Chemistry Department, Faculty of Science, Alexandria University, Alexandria, Egypt
- ² Materials Science Department, Institute of Graduate Studies and Research (IGSR), Alexandria University, Alexandria, Egypt